

Heterogeneous seismic anisotropy in the transition zone and uppermost lower mantle: evidence from South America, Izu-Bonin and Japan

Colton Lynner and Maureen D. Long

Department of Geology and Geophysics, Yale University, New Haven, CT 06511, USA. E-mail: colton.lynner@yale.edu

Accepted 2015 February 24. Received 2015 February 23; in original form 2014 December 20

SUMMARY

Measurements of seismic anisotropy are commonly used to constrain deformation in the upper mantle. Observations of anisotropy at mid-mantle depths are, however, relatively sparse. In this study we probe the anisotropic structure of the mid-mantle (transition zone and uppermost lower mantle) beneath the Japan, Izu-Bonin, and South America subduction systems. We present source-side shear wave splitting measurements for direct teleseismic *S* phases from earthquakes deeper than 300 km that have been corrected for the effects of upper mantle anisotropy beneath the receiver. In each region, we observe consistent splitting with delay times as large as 1 s, indicating the presence of anisotropy at mid-mantle depths. Clear splitting of phases originating from depths as great as ~ 600 km argues for a contribution from anisotropy in the uppermost lower mantle as well as the transition zone. Beneath Japan, fast splitting directions are perpendicular or oblique to the slab strike and do not appear to depend on the propagation direction of the waves. Beneath South America and Izu-Bonin, splitting directions vary from trench-parallel to trench-perpendicular and have an azimuthal dependence, indicating lateral heterogeneity. Our results provide evidence for the presence of laterally variable anisotropy and are indicative of variable deformation and dynamics at mid-mantle depths in the vicinity of subducting slabs.

Key words: Mantle processes; Seismic anisotropy; Dynamics of lithosphere and mantle; Pacific Ocean; South America.

INTRODUCTION

The transition zone is characterized by global seismic discontinuities in the mantle at 410 km and 660 km depth (e.g. Dziewonski & Anderson 1981; Helffrich 2000). The dominant mineral phases are wadsleyite in the upper transition zone (between 410 km and 520 km) and ringwoodite in the lower transition zone (between 520 km and 660 km). Below the 660 km discontinuity lies the lower mantle, whose dominant mineral phase is (Mg, Fe)SiO₃ perovskite, or bridgmanite (e.g. Bina & Wood 1987; Katsura & Ito 1989; Shearer 1990; Ita & Stixrude 1992; Tschauner *et al.* 2014). Globally, there is mixed evidence for the presence of seismic anisotropy at mid-mantle depths (transition zone and uppermost lower mantle), with some studies arguing for little to no anisotropy (e.g. Fischer & Wiens 1996; Kaneshima 2014), globally present anisotropy (Trampert & van Heijst 2002) or anisotropy only in the upper transition zone (e.g. Fouch & Fischer 1996; Fischer *et al.* 1998). In the vicinity of subducting slabs, evidence for anisotropy at mid-mantle depths from studies of shear wave splitting is accumulating (e.g. Wookey *et al.* 2002; Wookey & Kendall 2004; Foley & Long 2011; Di Leo *et al.* 2012; Lynner & Long 2014).

Measurements of seismic anisotropy offer relatively direct constraints on patterns of deformation in the mantle (e.g. Savage 1999; Long & Silver 2009). Seismic anisotropy arises from the alignment of anisotropic minerals when deformed via dislocation creep, developing a lattice preferred orientation, or LPO (e.g. Karato *et al.* 2008). Most shear wave splitting studies focus on the upper mantle, where olivine is the dominant anisotropic mineral and the relationships between strain and anisotropy are relatively well known (Karato *et al.* 2008). In deeper regions of the mantle, the relationship between strain and the resulting anisotropy is poorly understood. Despite this limitation, measurements of anisotropy at mid-mantle depths have the potential to offer significant insights into deep mantle dynamics.

Recently, progress has been made on several fronts in examining and interpreting mid-mantle anisotropy. Mineral physics experiments have shown that wadsleyite and ringwoodite are anisotropic (e.g. Tommasi *et al.* 2004; Mainprice 2007) and that wadsleyite can develop LPO and contribute to seismic anisotropy (Kawazoe *et al.* 2013). A recent geodynamical study by Faccenda (2014) suggested that the strains associated with subduction in the uppermost lower mantle are sufficiently large to align perovskite grains resulting

in anisotropy in the lower mantle. Numerical calculations of LPO development in polycrystalline MgSiO_3 perovskite (bridgmanite) suggest that fast directions of shear wave splitting would generally align with the direction of flow in the uppermost lower mantle (Mainprice *et al.* 2008). Observationally, several studies using the source-side shear wave splitting technique have found evidence for anisotropy at mid-mantle depths (Chen & Brudzinski 2003; Wookey & Kendall 2004; Foley & Long 2011; Di Leo *et al.* 2012; Lynner & Long 2014).

A limitation of these previously published studies is that they rely on limited ray path coverage and therefore offer poor azimuthal sampling, leaving our understanding of mid-mantle anisotropy patterns incomplete. Here we examine source-side shear wave splitting for events originating at transition zone depths beneath the Izu-Bonin, Japan and South American subduction systems. A primary goal is to explore whether these regions exhibit systematic lateral and/or azimuthal variations in splitting due to mid-mantle anisotropy, which would suggest laterally variable anisotropic structure. We therefore target the northwest Pacific and South American subduction systems, which both have abundant deep seismicity and excellent azimuthal coverage using seismic stations from global networks.

DATA AND METHODS

The source-side shear wave splitting technique uses direct S phases to probe anisotropy near the seismic source by first removing any effect from upper mantle anisotropy beneath the seismic station (e.g. Vinnik & Kind 1993; Russo & Silver 1994). As in most shear wave splitting studies, we assume the bulk of the lower mantle away from subducting slabs is isotropic as there should not be sufficient deformation to yield LPO development (Meade *et al.* 1995) and therefore attribute any splitting not accounted for by structure beneath the receiver to anisotropy near the source (near the subducting slab). Following Lynner & Long (2013, 2014), we select stations located 40° – 80° from the source regions for analysis. We have examined SK(K)S shear wave splitting patterns at each of the seismic stations used in this study to constrain receiver-side anisotropy. We restrict our analyses in this study to stations that exhibit simple patterns of shear wave splitting with sufficient backazimuthal coverage (at least two quadrants represented). Only stations characterized by null measurements (indicating an apparently isotropic upper mantle) or by consistent splitting (indicating a horizontal single layer of anisotropy) across a wide backazimuthal swath are used in this study. Stations with insufficient backazimuthal coverage or complex splitting that varies with backazimuth are not used (further details of receiver-side anisotropy corrections can be found in Lynner & Long 2014). This is a conservative approach that minimizes potential errors due to inaccurate receiver-side corrections through the selection of stations at which we are extremely confident in our characterization of the receiver-side anisotropic signal. While this approach limits the number of stations we can use in this study, our station distribution (Fig. 1 and Table S1) ensures good azimuthal coverage beneath both the northwest Pacific and South America (Fig. 1).

We selected earthquakes of magnitude $M_w > 5.0$ in both regions, restricting our analyses to events deeper than 300 km. Every seismogram was bandpass filtered between periods of 8 and 25 s; this filter is suitable for both the SK(K)S phases used to constrain the receiver-side corrections and the direct S waves used in the source-side splitting technique. We measured splitting parameters using Splitlab (Wüstefeld *et al.* 2008). Each waveform was visually in-

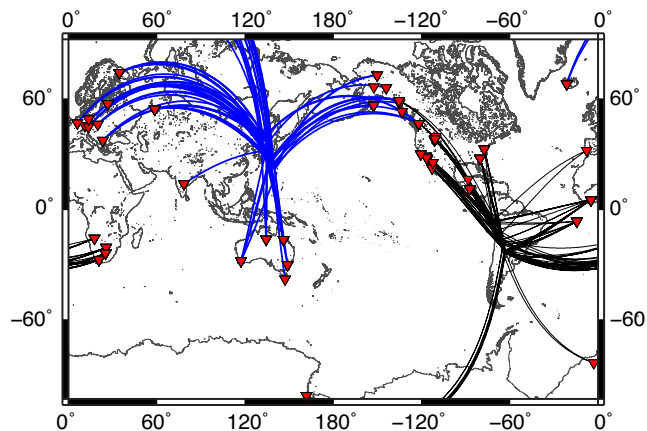


Figure 1. Map of the stations, red triangles, used in this study. Blue and black lines represent great circle paths connecting events and the stations at which those events yielded results for the northwest Pacific and South America, respectively.

spected to ensure good signal-to-noise ratios. At a few stations, we identified systematic polarization anomalies indicative of misalignments of the horizontal components (e.g. Tian *et al.* 2011) and corrected for these misalignments (Table S1).

We employed both the eigenvalue-minimization and rotation-correlation methods to determine the splitting parameters (fast direction, ϕ , and delay time, δt). The use of multiple measurement techniques ensures reliable results (e.g. Lynner & Long 2012). We only retained measurements for which results from the two methods were consistent, taking into account the 2σ error spaces. For simplicity, in this paper we report measurements from the rotation-correlation method. We required 2σ errors for ϕ and δt to be less than $\pm 25^\circ$ and ± 0.9 s, respectively. The non-weighted average errors in fast direction and delay time for the entire data set are 13.2° and 0.2 s, respectively. Null splitting measurements were classified as such based on linearity of S -wave particle motion after the effects of receiver-side anisotropy had been removed. In addition to the new measurements presented here, we also include previously published results from Japan (Lynner & Long 2014) made following the same criteria listed above.

RESULTS

Non-null splitting measurements for the northwest Pacific and South America are shown in Fig. 2; null splitting results are shown in Fig. S1. All measurements are plotted in a geographical reference frame relevant to the downgoing ray near the source. Beneath the northwest Pacific, the data set includes 113 null and 88 non-null measurements from 83 events at 29 stations; of these, 21 splits were previously published by Lynner & Long (2014). Beneath South America, we measured 68 split and 66 unsplit shear waves from 37 events at 23 different stations. All measured splitting parameters, with their estimated errors, can be found in Table S2.

All regions examined in this study exhibit significant splitting from deep earthquakes, with average delay times of ~ 1 s, as well as many null measurements. We primarily focus our interpretations on the clearly split measurements. (The null measurements are generally consistent with the observed fast splitting directions, in that their polarization directions often trend parallel or perpendicular to the fast directions, but they generally exhibit more scatter.) Beneath Japan and the southern Kurile arc, fast splitting directions generally

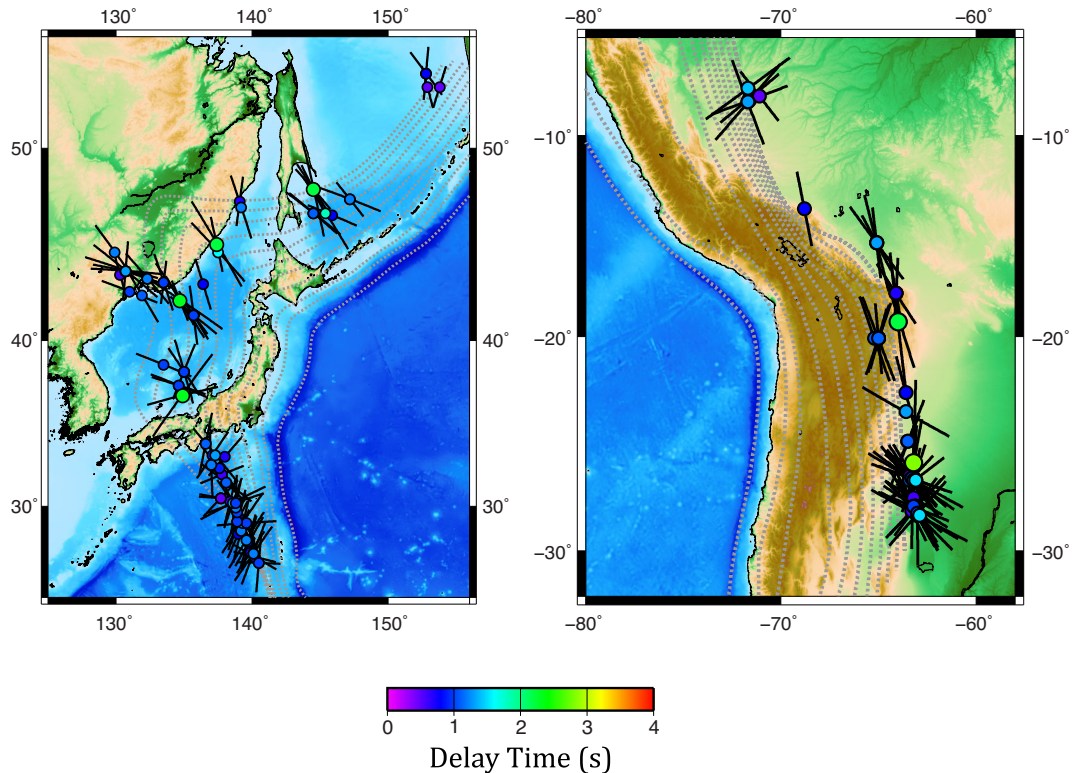


Figure 2. Source-side splitting results from events deeper than 300 km beneath the northwest Pacific (left-hand panel) and South America (right-hand panel). Fast directions have been projected back along the ray path to reflect the geometry of anisotropy in the mid-mantle beneath the seismic source sampled by the downgoing ray. Circles are plotted at event locations and the colour and size of the circle denote the largest delay time measured for that event. Orientations and lengths of the black bars correspond to fast directions and delay times, respectively. Dashed grey lines show slab contours at 50 km intervals from the compilation of Gudmundsson & Sambridge (1998).

trend in a NW–SE direction that aligns roughly normal to the strike of the trench and roughly parallel to the motion of the downgoing Pacific Plate (as do the null measurements). Beneath Izu-Bonin, the fast directions exhibit a less coherent pattern with highly scattered ϕ values. This scattered pattern is also mirrored by the null splitting observations. In both regions, the delay times exhibit little variation (Figs 2 and 3).

Beneath South America, we again observe splitting patterns that are geographically variable. In the southern portion (latitudes $\sim 25^\circ$ – 30° S), we observe variable fast splitting directions, while in the central portion of subduction zone (latitudes $\sim 12^\circ$ – 22° S) fast directions are consistently trench parallel. Beneath Peru, in the northernmost portion of the subduction system, we only obtained a few splitting measurements, but fast directions here follow either the strike of the trench or the motion of the downgoing plate. In all three of these areas, the null S arrivals generally follow similar trends but are characterized by more scatter than is observed for the split measurements. As with the northwest Pacific, we observe generally consistent delay times, with an average δt of ~ 0.9 s, Fig. 3.

A key question is whether the variability in observed fast directions beneath Izu-Bonin and southern South America represents systematic variations in apparent splitting as a function of azimuth, or merely scatter in the data. Fig. 4 shows the measured fast directions as a function of ray azimuth (with respect to trench strike) for three subregions, including the highly scattered regions of Izu-Bonin and southern South America, along with the Honshu region of Japan for comparison. These trends are also demonstrated in map view in Fig. 5 and in cross section in Fig. 6. For Izu-Bonin and South America, there is a clear and systematic variation of ϕ with ray ge-

ometry. For South America, rays that take off in the updip direction (to the northwest) exhibit average fast directions $\sim N15^\circ E$, while rays that take off in the downdip direction exhibit average ϕ values $\sim N50^\circ W$. Beneath Izu-Bonin, we observe a cluster of rays that take off to the south (in a downdip direction close to the strike of the trench) that exhibit fast directions that are $\sim N70^\circ W$, while a group of rays that take off to the northwest (along strike) and northeast (updip) exhibit fast directions $\sim N20^\circ E$ and $\sim N30^\circ W$, respectively. In contrast, beneath Honshu there is considerably less scatter in the observed fast directions, with no systematic trends.

DISCUSSION

An important feature of this data set is the observation of splitting (delay times ~ 0.8 s) from events that originate as deep as ~ 600 km beneath both the northwestern Pacific and South American regions. While measurements originating from depths greater than ~ 600 km are relatively sparse, they are present in each region and are well-resolved measurements. This robust observation argues for the presence of anisotropy in the uppermost lower mantle as well as at transition zone depths (Fig. 3). Interestingly, there does not appear to be a strong dependence of delay time (or ϕ) on depth, suggesting that anisotropy in the uppermost lower mantle may account for the bulk of the splitting signal. In all regions examined in this study, we observe splitting for events that originate beneath the wadsleyite stability field, so LPO of wadsleyite alone cannot be a primary explanation. Ringwoodite, the most volumetrically important mineral in the lower transition zone, is anisotropic (~ 4 – 8 per cent V_s anisotropy; e.g. Wang *et al.* 2006; Mainprice 2007), but is

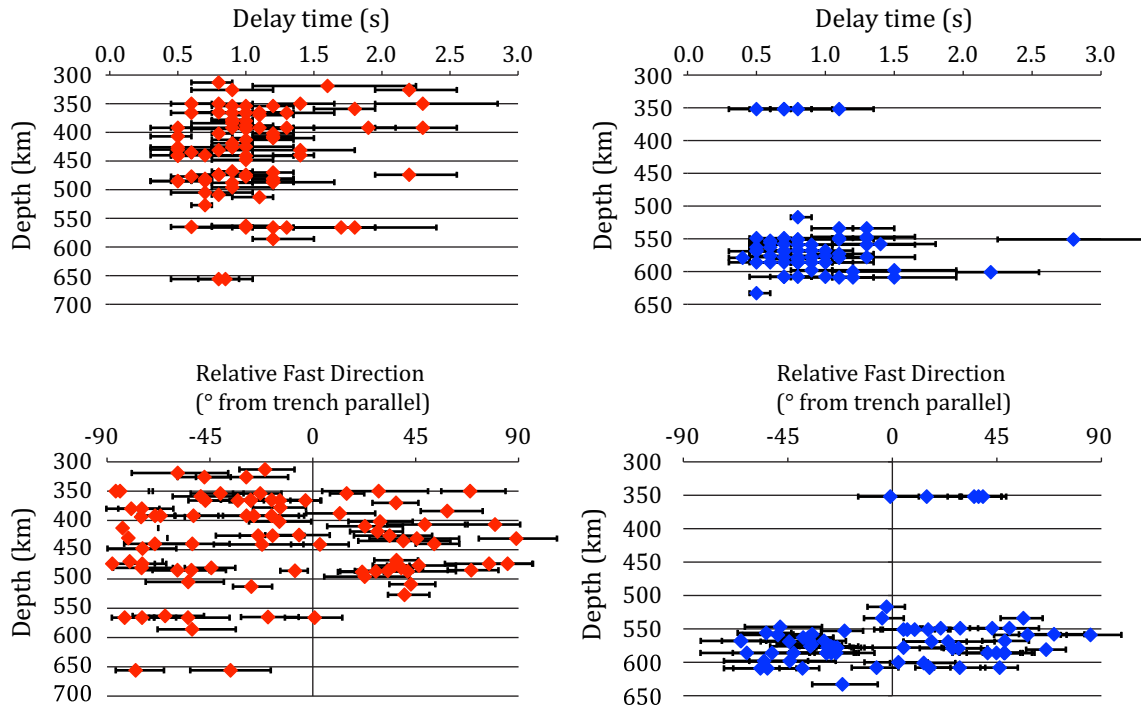


Figure 3. Plots of delay time (top panels) and fast direction relative to the local strike of the trench (bottom panels) versus event depth for the northwestern Pacific (left-hand panels, red) and South American (right-hand panels, blue) subduction systems. Error bars denote the 2σ errors associated with each measurement.

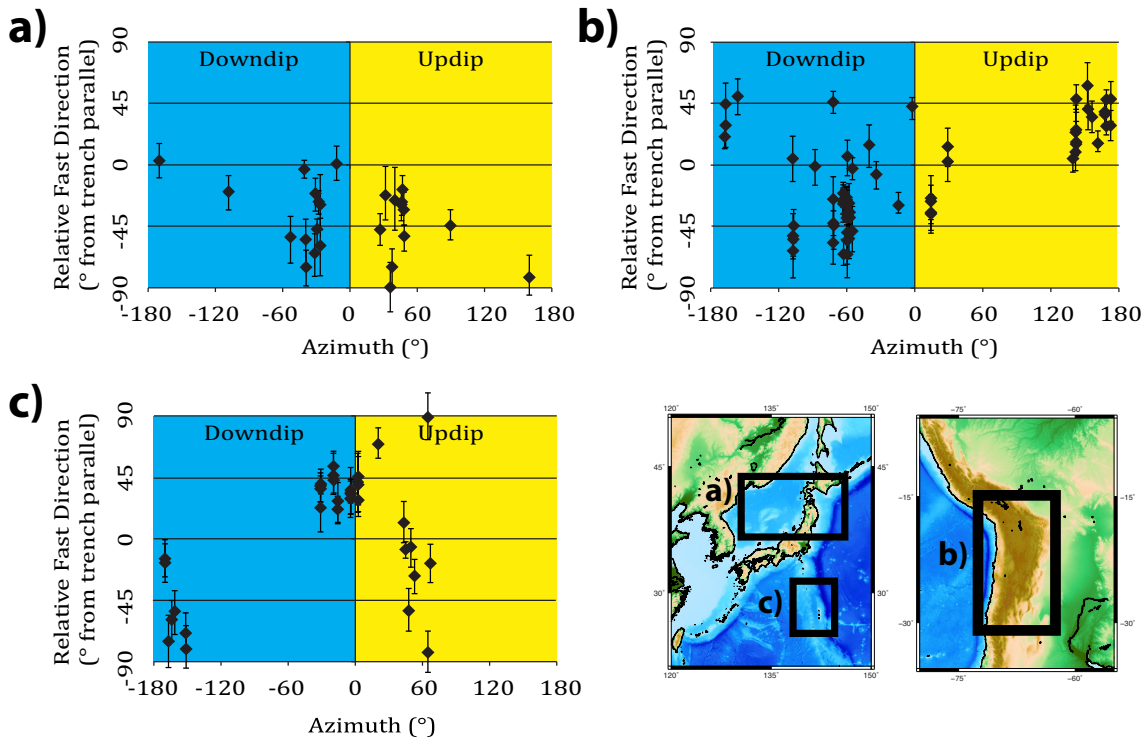


Figure 4. Plots of measured fast directions (diamonds) versus ray azimuth relative to local trench strike for source-side measurements made beneath Japan (a), southern South America (b) and southern Izu-Bonin (c), as shown in the inset map. The green diamond represents a fast direction plotted at its equivalent negative value.

also an unlikely primary explanation for our observations, as events as deep as ~ 600 km yield large delay times. Rays originating at ~ 600 km depth cannot sample enough transition zone material to accrue the observed ~ 0.8 s of splitting.

We therefore propose that the most likely mechanism for our observations is LPO of perovskite in the uppermost lower mantle (given that the volume fraction of MgO is only ~ 10 per cent; e.g., Mainprice 2007), perhaps with a small additional contribution from

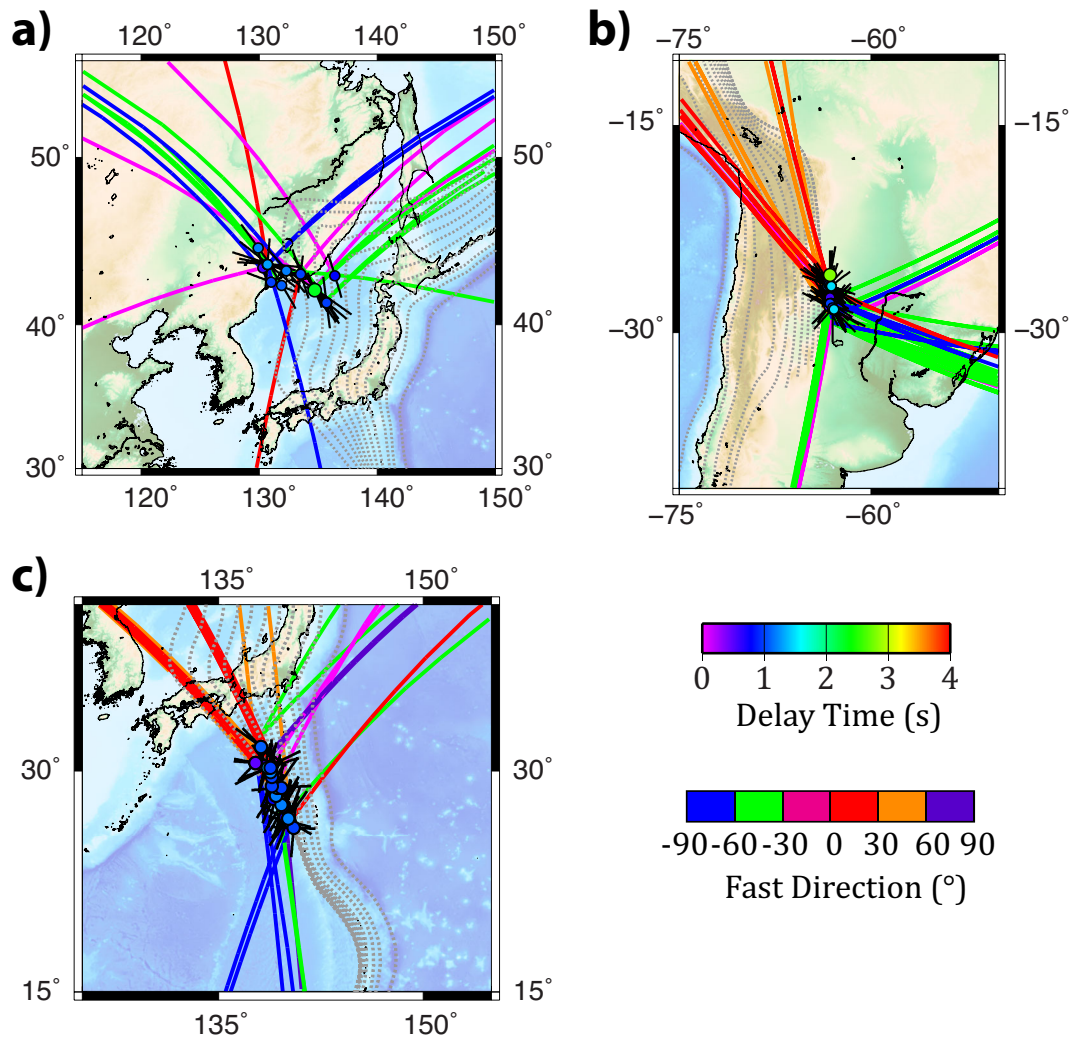


Figure 5. Plots of ray paths for measurements made beneath Japan (a), southern South America (b) and southern Izu-Bonin (c). Circles, black lines, and slab contours are plotted following the same conventions as Fig. 2. Thick coloured lines represent ray paths of the different splitting measurements in each region as seen from above. The colours of the lines denote the measured fast direction associated with a given ray path, as shown in the legend at the bottom right-hand side.

anisotropy in the transition zone. Perovskite is anisotropic at lower mantle pressures (~ 10 per cent V_s anisotropy; Wentzcovitch *et al.* 2004) and deviatoric stresses may be sufficient to deform the uppermost lower mantle around subducting slabs via dislocation creep (Cordier *et al.* 2004), thus generating LPO (Mainprice *et al.* 2008; Faccenda 2014).

While we suggest that LPO of MgSiO_3 perovskite represents the most likely primary explanation for our observations, other mineral phases, such as dense hydrous phases, may also play some role in generating mid-mantle anisotropy (e.g. Rosa *et al.* 2013; Nowacki *et al.* 2014), but are unlikely as primary mechanisms for the observed anisotropy. Phase D, a dense hydrous magnesium-silicate phase, is substantially more anisotropic (~ 18 per cent V_s anisotropy) than perovskite and is stable throughout the upper lower mantle (Mainprice *et al.* 2007; Mainprice & Ildefonse 2009). Phase D, however, should be confined to hydrated regions such as the relatively cool interiors of subducting slabs. If LPO of phase D (or any other source of anisotropy confined to the slab) was the primary source of anisotropy in the mid-mantle, there should be a systematic trend in delay time with the amount of slab material being sampled, which is not observed (Fig. S2). If the anisotropy were confined

to subducting slabs, rays sampling large volumes of slab material would show larger delay times than those sampling little slab material (with some dependence on the orientation of anisotropy). This would result in larger delay times for rays traveling in a downdip direction than for those in an updip direction. Such a trend in delay time is not observed in our data set, however. This lack of trend is particularly obvious beneath South America, where rays traveling to the east (in a downdip direction) sample long paths (100 s of km) of slab material, while those traveling to the northwest (in an updip direction) sample little slab material (< 100 km). Despite this difference in slab sampling, all rays exhibit similar delay times (Fig. 5 and Fig. S2) arguing against slab anisotropy as a primary explanation for our observations.

Another striking feature of this data set is the geographic variability we observe in the geometry of mid-mantle anisotropy, both between different subduction systems and within individual regions. Beneath Honshu and the central portion of South America, we observe fast splitting directions that do not vary significantly with azimuth (Fig. 2), despite having similar azimuthal coverage as the variable regions, Fig. 5. However, there is a pronounced difference in geometry between the two systems: beneath Honshu, ϕ values

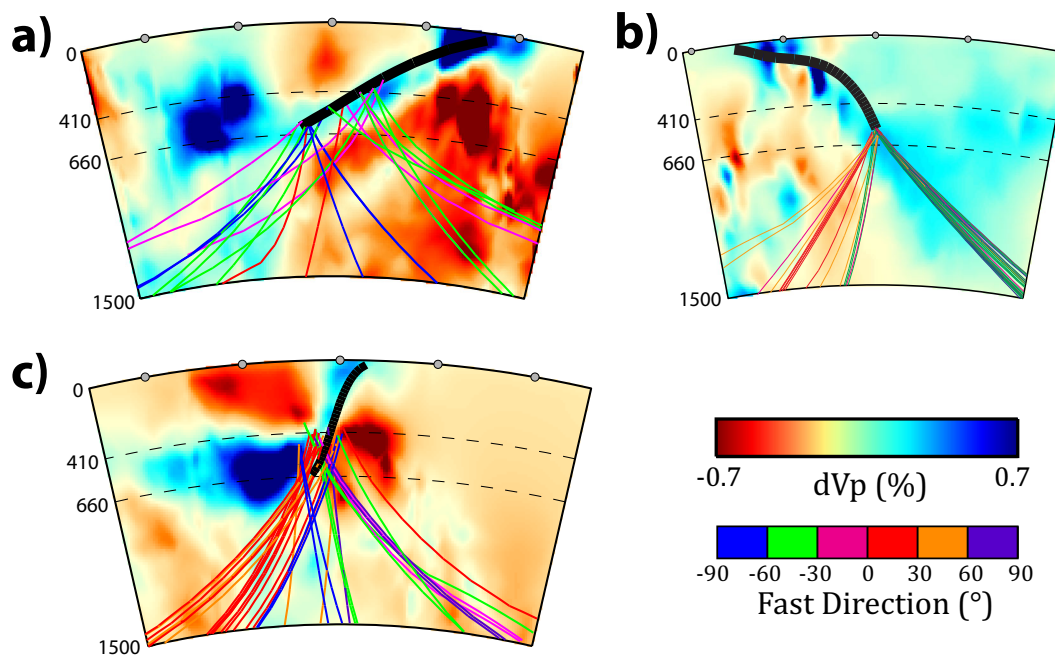


Figure 6. Ray paths plotted on top of isotropic P velocity anomalies (as indicated by the colour bar) from the tomographic model of Li *et al.* (2008) for Japan (a), southern South America (b) and southern Izu-Bonin (c). Colours of the ray paths follow the same conventions at Fig. 5. Thick black lines represent the slab contours from Gudmundsson & Sambridge (1998).

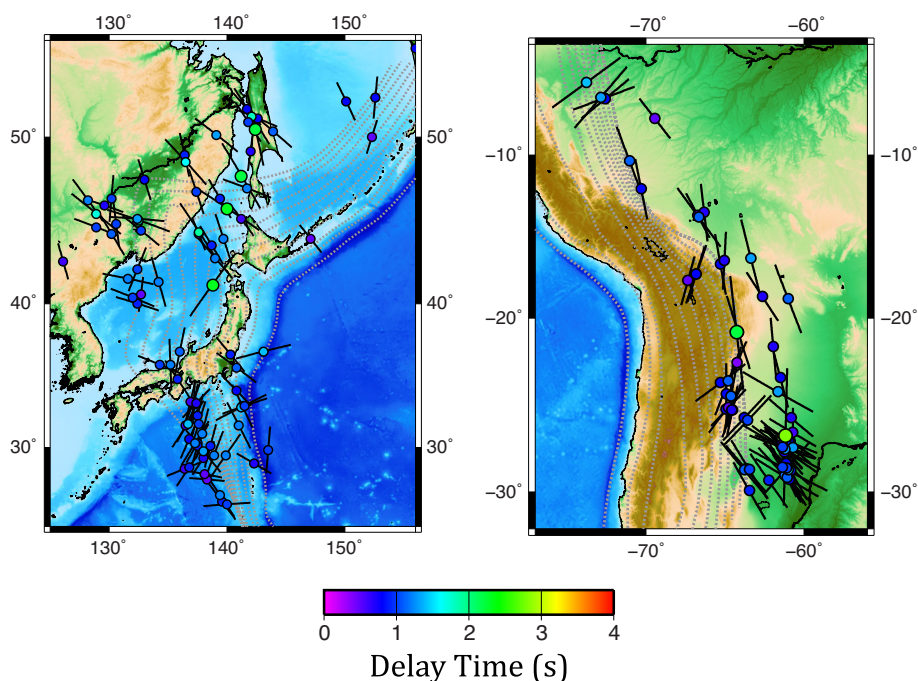


Figure 7. Same as Fig. 2, except that source-side splitting results are plotted at 800 km (uppermost lower mantle) pierce points for each downgoing ray. Ray paths were calculated using Tau P (Crowell *et al.* 1999) with the isap91 earth model (Kennett & Engdahl 1991). Other plotting conventions are the same as in Fig. 2.

tend to align with the motion of the downgoing plate, while beneath central South America, fast directions generally align with the strike of the trench. Beneath Izu-Bonin and southern South America, the systematic variability in observed fast directions as a function of ray azimuth (Figs 4–6) suggests laterally heterogeneous deformation in the uppermost lower mantle within the subduction system. This

is illustrated further in Fig. 7, which shows the splitting observations beneath both regions plotted at 800 km deep pierce points (in the uppermost lower mantle) for each ray. When plotted using this convention, the variable splitting observations separate into distinct coherent groups, supporting the notion that the primary source of anisotropy is in the uppermost lower mantle and providing further

support to our interpretation of laterally heterogeneous mid-mantle anisotropy.

Beneath southern South America, rays that travel northwestward show roughly trench parallel fast directions (similar to the splitting seen in the central portion of South America), but rays that sample in an eastward (downdip) and southward direction (along strike) are marked by very different fast splitting directions (Figs 5 and 6). When the observations are plotted at 800 km depth (Fig. 7), the splitting measurements tend to group into regions of coherent splitting. In the southernmost area, the splitting is trench oblique (roughly paralleling the motion of the downgoing slab), while the rest of the southern and central South America shows trench parallel orientations. This heterogeneous splitting pattern indicates laterally heterogeneous anisotropy beneath southernmost South America, likely indicating variable deformation geometry of the slab itself and/or the subslab mantle. Experimental constraints on the relationship between LPO development and mantle flow for mid-mantle minerals are absent, but first-principles calculations of the glide systems of bridgmanite have been carried out (Mainprice *et al.* 2008). This work suggests that the LPO of polycrystalline bridgmanite in the uppermost lower mantle would result in fast splitting directions that roughly align with the direction of shear. This would suggest that in the southernmost region of South America, mid-mantle deformation likely corresponds to 2-D entrainment of the subslab lower mantle with the downgoing slab, while beneath the rest of South America the observations are more consistent with trench parallel flow.

Beneath Izu-Bonin, the splitting pattern is even more complicated, with rays traveling southward (downdip, nearly along strike) having a different ϕ than either those that head to the northeast (along strike) or northwest (updip), again indicating laterally varying deformation beneath the slab. In this region, a possible scenario for the geometry of mantle flow and deformation is different beneath the portion of the slab that has stagnated atop the 660 km discontinuity and the shallower portion where the slab is subducting normally (Figs 6 and 7) arguing for variable subslab dynamics. The southernmost portion of Izu-Bonin is characterized by trench-parallel splitting and therefore (using the relationship between strain anisotropy for bridgmanite described above) trench parallel flow. In contrast, the rest of the subduction zone is characterized by variable, largely trench-oblique fast orientations, consistent with variable deformation geometries beneath the slab. These inferences also contrast with observations beneath Japan, which suggest generally entrained mantle flow beneath the subducting slab, despite the fact that both regions experience slab deflection atop the 660 km discontinuity. As with southern South America, laterally varying deformation of mid-mantle material beneath Izu-Bonin can account for the azimuthal variation in source-side splitting, while beneath Japan the dynamic regime appears to be simpler.

CONCLUSION

Source-side shear wave splitting measurements for rays originating below 350 km beneath the Japan/Kurile, Izu-Bonin, and South America subduction systems reveal significant anisotropy (with ~ 1 s delay times) at mid-mantle depths. In combination with previously published observations (Wookey *et al.* 2002; Chen & Brudzinski 2003; Foley & Long 2011; Di Leo *et al.* 2012; Lynner & Long 2014), our measurements suggest that mid-mantle anisotropy in subduction systems is likely a global feature. Furthermore, our observation of consistent splitting with delay times ~ 0.8 s for events as deep as ~ 600 km indicates the presence of anisotropy in the

uppermost lower mantle as our observations cannot be explained only in terms of anisotropy at transition zone depths. A likely mechanism for anisotropy in the uppermost lower mantle is deformation in the dislocation creep regime at high deviatoric stresses induced by slabs impinging on the high-viscosity lower mantle, resulting in LPO of MgSiO₃ perovskite (Faccenda 2014). We observe generally consistent delay times in all regions examined in this study, suggesting that the magnitude of mid-mantle anisotropy is uniform. In contrast, we observe striking variations in measured fast splitting directions, both between and within individual subduction systems. Beneath southern South America and Izu-Bonin, we have documented systematic variations in ϕ with azimuth, while beneath central South America and Japan measured fast directions do not vary with azimuth. Our observations suggest that mid-mantle deformation is heterogeneous, indicating lateral variations in mid-mantle dynamics beneath subducting slabs, especially beneath southern South America and Izu-Bonin. Our measurements suggest that subducting slabs play an important role in deforming the surrounding mantle as they sink into the deeper portions of the mantle, and that the deformation patterns are heterogeneous both within and among individual subduction systems.

ACKNOWLEDGEMENTS

This work was funded by NSF grant EAR-1150722. Figures were prepared using Generic Mapping Tools (Wessel & Smith 1991). We used seismic data from Global Seismograph Network (II, IU), Global Telemetered Seismic Network (GT), United States National Seismic Network (US), Caltech Regional Seismic Network (CI), Alaska Regional Network (AK), Alaska Tsunami Warning Seismic System (AT), Czech Regional Seismic Network (CZ), Caribbean Network (CU), NARS Array (NR), Polish Seismological Network (PL), German Regional Seismic Network (GR), Portuguese National Seismic Network (PM), Netherlands Seismic Network (NL), Canadian National Seismic Network (CN), Intermountain West (IW), Mednet (MN), Geoscope (G) and Geofon (GE) networks. All waveforms were downloaded from the Data Management Center (DMC) of the Incorporated Research Institutions for Seismology (IRIS).

REFERENCES

- Bina, C.R. & Wood, B.J., 1987. Olivine–spinel transitions: experimental and thermodynamic constraints and implications for the nature of the 400-km seismic discontinuity, *J. geophys. Res.*, **92**(B6), 4853–4866.
- Chen, W.-P. & Brudzinski, M.R., 2003. Seismic anisotropy in the mantle transition zone beneath Fiji-Tonga, *Geophys. Res. Lett.*, **30**, 1682, doi:10.1029/2002GL016330.
- Cordier, P., Ungár, T., Zsoldos, L. & Tichy, G., 2004. Dislocation creep in MgSiO₃ perovskite at conditions of the Earth's uppermost lower mantle, *Nature*, **428**(6985), 837–840.
- Crotwell, H.P., Owens, T.J. & Ritsema, J., 1999. The TauP toolkit: flexible seismic travel-time and ray-path utilities, *Seismol. Res. Lett.*, **70**, 154–160.
- Di Leo, J.F., Wookey, J., Hammond, J.O.S., Kendall, J.-M., Kaneshima, S., Inoue, H., Yamashina, T. & Harjadi, P., 2012. Mantle flow in regions of complex tectonics: insights from Indonesia, *Geochem. Geophys. Geosyst.*, **13**, Q12008, doi:10.1029/2012GC004417.
- Dziewonski, A.M. & Anderson, D.L., 1981. Preliminary reference Earth model, *Phys. Earth planet. Int.*, **25**(4), 297–356.
- Faccenda, M., 2014. Mid mantle seismic anisotropy around subduction zones, *Phys. Earth planet. Inter.*, **227**, 1–19.
- Fischer, K.M. & Wiens, D.A., 1996. The depth distribution of mantle anisotropy beneath the Tonga subduction zone, *Earth planet. Sci. Lett.*, **142**(1), 253–260.

- Fischer, K.M., Fouch, M.J., Wiens, D.A. & Boettcher, M.S., 1998. Anisotropy and flow in Pacific subduction zone back-arcs, *Pure appl. Geophys.*, **151**(2–4), 463–475.
- Foley, B.J. & Long, M.D., 2011. Upper and mid-mantle anisotropy beneath the Tonga slab, *Geophys. Res. Lett.*, **38**, L02303, doi:10.1029/2010GL046021.
- Fouch, M.J. & Fischer, K.M., 1996. Mantle anisotropy beneath northwest Pacific subduction zones, *J. geophys. Res.*, **101**(B7), 15 987–16 002.
- Gudmundsson, O. & Sambridge, M., 1998. A regionalized upper mantle (RUM) seismic model, *J. geophys. Res.*, **103**, 7121–7136.
- Helfrich, G., 2000. Topography of the transition zone seismic discontinuities, *Rev. Geophys.*, **38**(1), 141–158.
- Ita, J. & Stixrude, L., 1992. Petrology, elasticity, and composition of the mantle transition zone, *J. geophys. Res.*, **97**(B5), 6849–6866.
- Kaneshima, S., 2014. Upper bounds of seismic anisotropy in the Tonga slab near deep earthquake foci and in the lower mantle, *Geophys. J. Int.*, **197**, 351–368.
- Karato, S., Jung, H., Katayama, I. & Skemer, P., 2008. Geodynamic significance of seismic anisotropy of the upper mantle: new insights from laboratory studies, *Annu. Rev. Earth planet Sci.*, **36**, 59–95.
- Katsura, T. & Ito, E., 1989. The system Mg₂SiO₄–Fe₂SiO₄ at high pressures and temperatures: precise determination of stabilities of olivine, modified spinel, and spinel, *J. geophys. Res.*, **94**(B11), 15 663–15 670.
- Kawazoe, T., Ohuchi, T., Nishihara, Y., Nishiyama, N., Fujino, K. & Irifune, T., 2013. Seismic anisotropy in the mantle transition zone induced by shear deformation of wadsleyite, *Phys. Earth planet. Inter.*, **216**, 91–98.
- Kennett, B.L.N. & Engdahl, E.R., 1991. Traveltimes for global earthquake location and phase identification, *Geophys. J. Int.*, **105**, 429–465.
- Li, C., van der Hilst, R.D., Engdahl, E.R. & Burdick, S., 2008. A new global model for P wave speed variations in Earth's mantle, *Geochem. Geophys. Geosyst.*, **9**(5) Q05018, doi:10.1029/2007GC001806.
- Long, M.D. & Silver, P.G., 2009. Shear wave splitting and mantle anisotropy: measurements, interpretations, and new directions, *Surv. Geophys.*, **30**, 407–461.
- Lynner, C. & Long, M.D., 2012. Evaluating contributions to SKKS splitting from lower mantle anisotropy: a case study from station DBIC, Côte D'Ivoire, *Bull. seism. Soc. Am.*, **102**, 1030–1040.
- Lynner, C. & Long, M.D., 2013. Sub-slab seismic anisotropy and mantle flow beneath the Caribbean and Scotia subduction zones: effects of slab morphology and kinematics, *Earth planet. Sci. Lett.*, **361**, 367–378.
- Lynner, C. & Long, M.D., 2014. Sub-slab anisotropy beneath the Sumatra and circum-Pacific subduction zones from source-side shear wave splitting observations, *Geochem. Geophys. Geosyst.*, **15**, 2262–2281.
- Mainprice, D., 2007. Seismic anisotropy of the deep Earth from a mineral and rock physics perspective, *Treatise Geophys.*, **2**, 437–491.
- Mainprice, D. & Ildefonse, B., 2009. Seismic anisotropy of subduction zone minerals—contribution of hydrous phases, in *Subduction Zone Geodynamics*, pp. 63–84, eds Lallemand, S. & Funicello, F., Springer-Verlag.
- Mainprice, D., LePage, Y., Rodgers, J. & Jouanna, P., 2007. Predicted elastic properties of the hydrous D phase at mantle pressures: implications for the anisotropy of subducted slabs near 670-km discontinuity and in the lower mantle, *Earth planet. Sci. Lett.*, **259**(3), 283–296.
- Mainprice, D., Tommasi, A., Ferré, D., Carrez, P. & Cordier, P., 2008. Predicted glide systems and crystal preferred orientations of polycrystalline silicate Mg-Perovskite at high pressure: implications for the seismic anisotropy in the lower mantle, *Earth planet. Sci. Lett.*, **271**(1), 135–144.
- Meade, C., Silver, P.G. & Kaneshima, S., 1995. Laboratory and seismological observations of lower mantle isotropy, *Geophys. Res. Lett.*, **22**, 1293–1296.
- Nowacki, A., Kendall, J.-M., Wookey, J. & Permberton, A., 2014. Transition zone anisotropy beneath deep slabs and the transport of water into the lower mantle, in *Proceeding of the AGU Fall Meeting*, Abstract: D141B-4333.
- Rosa, A.D., Mezouar, M., Garbarino, G., Bouvier, P., Ghosh, S., Rohrbach, A. & Sanchez-Valle, C., 2013. Single-crystal equation of state of phase D to lower mantle pressures and the effect of hydration on the buoyancy of deep subducted slabs, *J. geophys. Res.*, **118**, 6124–6133.
- Russo, R.M. & Silver, P.G., 1994. Trench-parallel flow beneath the Nazca Plate from seismic anisotropy, *Science*, **263**, 1105–1111.
- Savage, M.K., 1999. Seismic anisotropy and mantle deformation: what have we learned from shear wave splitting, *Rev. Geophys.*, **37**, 65–106.
- Shearer, P.M., 1990. Seismic imaging of upper-mantle structure with new evidence for a 520-km discontinuity, *Nature*, **344**(6262), 121–126.
- Tian, X., Zhang, J., Si, S., Wang, J., Chen, Y. & Zhang, Z., 2011. SKS splitting measurements with horizontal component misalignment, *Geophys. J. Int.*, **185**, 329–340.
- Tommasi, A., Mainprice, D., Cordier, P., Thoraval, C. & Couvy, H., 2004. Strain-induced seismic anisotropy of wadsleyite polycrystals and flow patterns in the mantle transition zone, *J. geophys. Res.*, **109**, B12405, doi:10.1029/2004JB003158.
- Trampert, J. & van Heijst, H.J., 2002. Global azimuthal anisotropy in the transition zone, *Science*, **296**(5571), 1297–1299.
- Tschauner, O., Ma, C., Beckett, J.R., Prescher, C., Prakapenka, V.B. & Rossman, G.R., 2014. Discovery of bridgmanite, the most abundant mineral in Earth, in a shocked meteorite, *Science*, **346**(6213), 1100–1102.
- Vinnik, L.P. & Kind, R., 1993. Ellipticity of teleseismic S-particle motion, *Geophys. J. Int.*, **113**(1), 165–174.
- Wang, J., Sinogeikin, S.V., Inoue, T. & Bass, J.D., 2006. Elastic properties of hydrous ringwoodite at high-pressure conditions, *Geophys. Res. Lett.*, **33**(14), doi:10.1029/2006GL026441.
- Wentzcovitch, R.M., Karki, B.B., Cococcioni, M. & de Gironcoli, S., 2004. Thermoelastic properties of MgSiO₃ perovskite: insights on the nature of the Earth's lower mantle, *Phys. Rev. Lett.*, **92**, 018501, doi:10.1103/PhysRevLett.92.018501.
- Wessel, P. & Smith, W.H.F., 1991. Free software helps map and display data, *EOS, Trans. Am. geophys. Un.*, **72**, 441–446.
- Wookey, J. & Kendall, J.-M., 2004. Evidence of mid-mantle anisotropy from shear wave splitting and the influence of shear-coupled P waves, *J. geophys. Res.*, **109**, B07309, doi:10.1029/2003JB002871.
- Wookey, J., Kendall, J.-M. & Barruol, G., 2002. Mid-mantle deformation inferred from seismic anisotropy, *Nature*, **415**(6873), 777–780.
- Wüstefeld, A., Bokelmann, G., Barruol, G. & Zaroli, C., 2008. Splitlab: a shear-wave splitting environment in Matlab, *Comp. Geosci.*, **34**, 515–528.

SUPPORTING INFORMATION

Additional Supporting Information may be found in the online version of this paper:

Table S1. Station misalignment and receiver-side anisotropy corrections for the stations used in this study.

Table S2. Source-side shear wave splitting results and associated errors for South America, Izu-Bonin, and Japan.

Figure S1. Null splitting results from the northwest Pacific and South America. Circles are plotted at the event location. The bars correspond to the two possible orientations, either the polarization of the fast or the slow directions of anisotropy, of the null split ray calculated from the initial polarization of the incoming S wave. Nulls are plotted in relation to their orientation in the source-side mantle.

Figure S2. Delay time versus ray azimuth for measurements beneath Japan (a), South America (b) and Izu-Bonin (c). There is a lack of azimuthal variation in delay time beneath South American and Izu-Bonin despite the azimuthal variation in fast direction. (<http://gji.oxfordjournals.org/lookup/suppl/doi:10.1093/gji/ggv099/-/DC1>)

Please note: Oxford University Press is not responsible for the content or functionality of any supporting materials supplied by the authors. Any queries (other than missing material) should be directed to the corresponding author for the paper.